

Figure S1, related to Figure 1:

(A): Expression level of HKII, PDHB, COXI in CAFs and NOFs. (B): Representative IHC images showing protein expression of GLUL, GOT2, BCAT1 for NOFs and CAFs. (C): Relative expression of GLUL, GOT2, BCAT1 in CAFs compared to NOFs. (D-F): Clustermap of expression of genes encoding glycolysis (D), glutamine metabolism (E) and ETC (F) enzymes in microdissected NOFs (NS samples) and CAFs (TS samples) derived from ovarian cancer patients. In ETC, the genes are listed as order from top to bottom: NDUFA5, ATP5L, ATP6V1, DAP6V1, DNDUFS8, ATP5G2, NDUFA11, COX6B1, COX6A1, CYC1, NDUFB9, ATP6V0B, ATP5G3, ATP6AP1, ATP6V1H, NDUFS3, ATP6V0E1, NDUFS1, UQCRFS1, UQCRC1, ATP5B, NDUFA10, SDHB, ATP6V1C1, PPA1, ATP5G3, ATP5O, ATP5C1, ATP5F1, ATP6V1C1, COX11, NDUFB10, ATP5D, ATP5I, ATP5E, NDUFA11, UQCR11, NDUFB2, ATP5A1, NDUFB5, NDUFA8, COX5A, UQCRH, NDUFA2, UQCRC2, NDUFC1, NDUFA6, NDUFB2, NDUFB8, ATP6V1A, SDHD, COX6C, ATP5J, NDUFC2, NDUFB4, COX8A, NDUFS6, NDUFAB1, NDUFV2, COX5B, ATP5J2, NDUFA9, NDUFA3, COX17, UQCRQ, ATP6V0E1, ATP6V1G1, PPA2, ATP5L, NDUFA4, COX7A2, ATP5O, ATP6V0E1, COX7C, NDUFB1, COX7B, NDUFB6, UQCRB, UQCRB1, COX4I1, COX4I, NDUFB3, COX7A2L, SDHC, NDUFS2, NDUFA1, NDUFA6, ATP6V0D1, ATP6V1E1, SDHAF1, ATP6V0, CATP5H, ATP6V1F, ATP5G1, NDUFV3, NDUFS8, NDUFA7, NDUFB7, NDUFB10, NDUFS7, UQCR10, NDUFV1, ATP6V0E2, NDUFV3, NDUFS1, ATP6V1G1, UQCRB, NDUFS1, COX15, COX1, COX2, COX2, ATP6ND2, COX3. (G): Average expression of glycolysis genes in paired tumor epithelial and stromal compartments. Lines connecting tumor and stromal data points signify tumor and stromal samples derived from the same patient (Wisconsin test). (H): Doubling time of various NOFs and CAFs in complete medium. For all graphs, error bars indicate mean \pm s.e.m. for $n \geq 3$ independent experiments. Two tailed student t-test if not indicated.

A

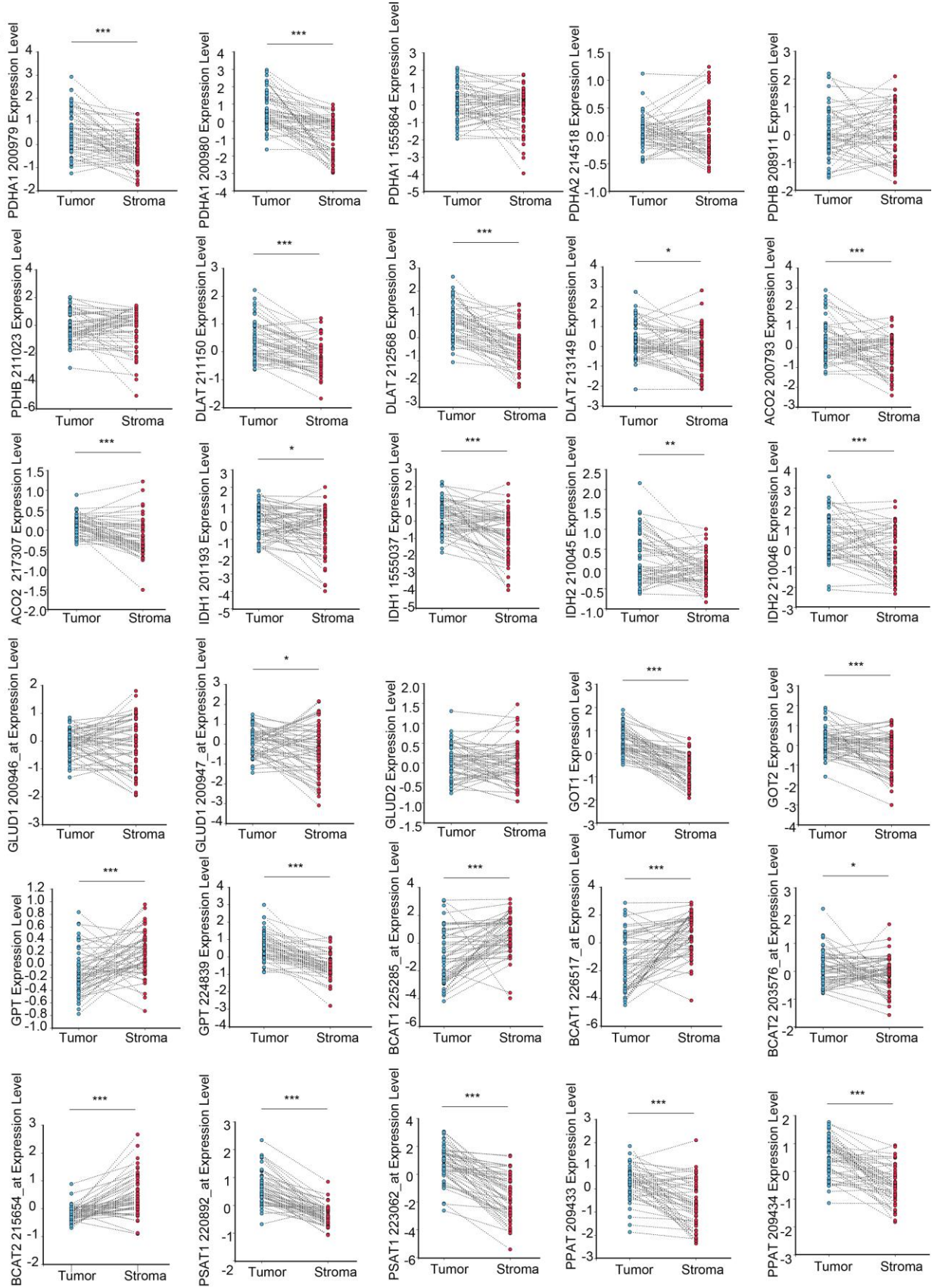


Figure S2, related to Figure 1:

(A): Expression of genes encoding central carbon metabolic enzymes in paired tumor epithelial and stromal compartments. Lines connecting tumor and stromal data points signify tumor and stromal samples derived from the same patient. n=33. (Wilcoxin test).

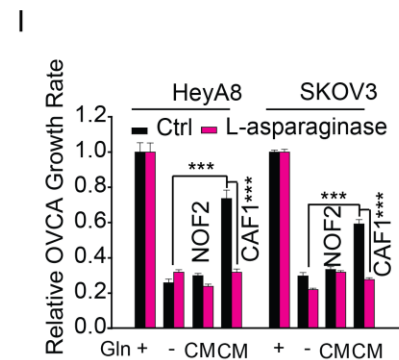
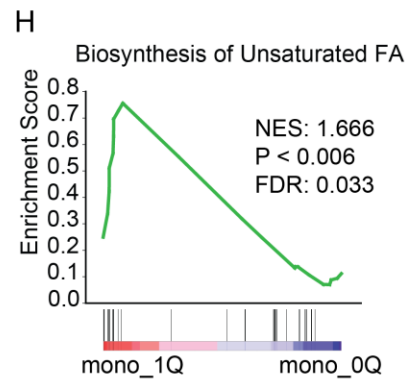
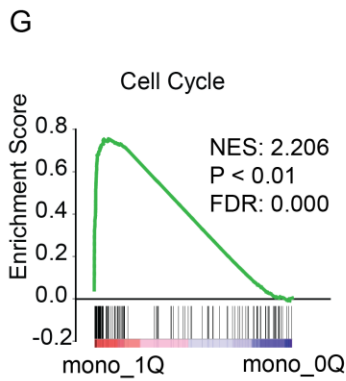
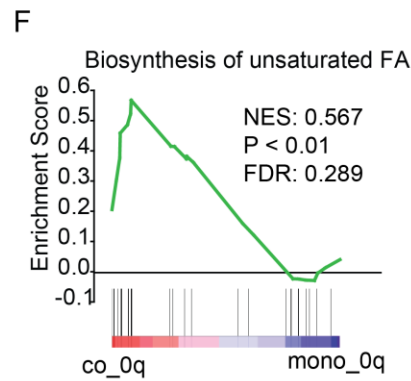
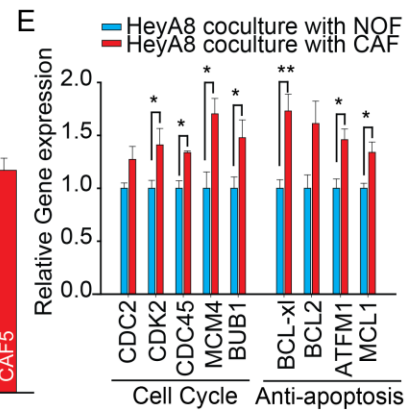
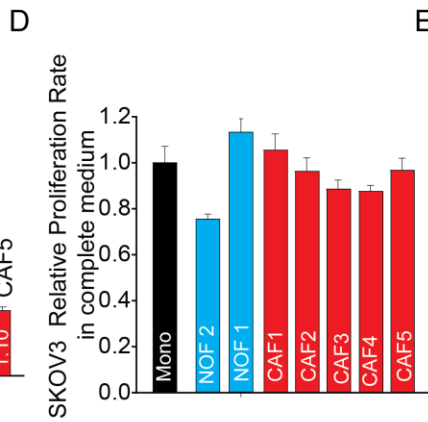
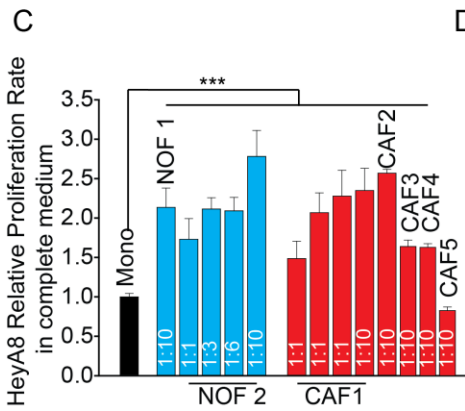
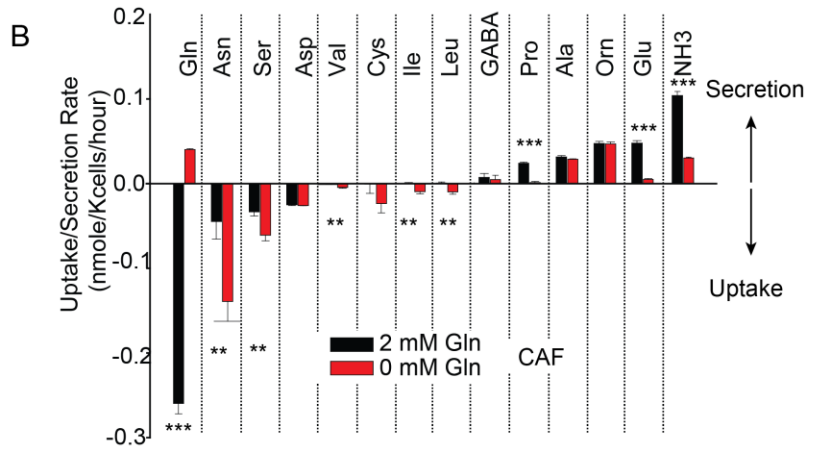
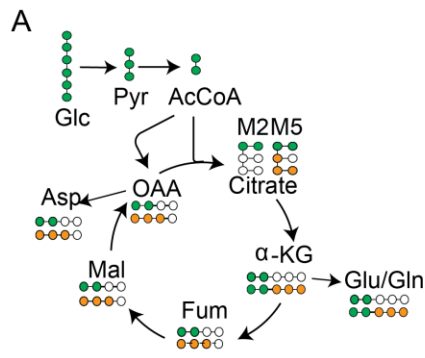


Figure S3, related to Figure 2 and Figure 3:

(A): Schematic showing fate of U-¹³C glucose enriching TCA cycle metabolites. (B): Extracellular fluxes of amino acids in CAF1 cells in Gln-deprived and nutrient-rich medium. (C-D): The effect of CAFs or NOFs on the proliferation rate of HeyA8 (C) and SKOV3 (D) in complete medium. (E): The relative expression level of genes related to cell cycle and anti-apoptosis in HeyA8 when cells are cocultured with CAFs, compared to cells cocultured with NOFs. (F): Gene set enrichment analysis (GSEA) of unsaturated fatty acid biosynthesis genes in Gln-deprived HeyA8 when transwell co-cultured with CAFs with respect to mono-cultured HeyA8 in Gln deprived medium. Gene expression are measured 48 hours after culturing in respective media. (G-H) GSEA of cell cycle (G) and unsaturated fatty acid biosynthesis (H) genes in mono-cultured HeyA8 in nutrient-rich medium with respect to mono-cultured HeyA8 in Gln deprived medium. Gene expression are measured 48 hours after culturing in respective media. (I): Growth rate of HeyA8 and SKOV3 cultured in condition medium from NOF or CAF and treated with L-asparaginase relative to HeyA8 or SKOV3 in nutrient-rich media. Error bars indicate mean \pm s.e.m. for $n \geq 3$ independent experiments. Two tailed student t-test.

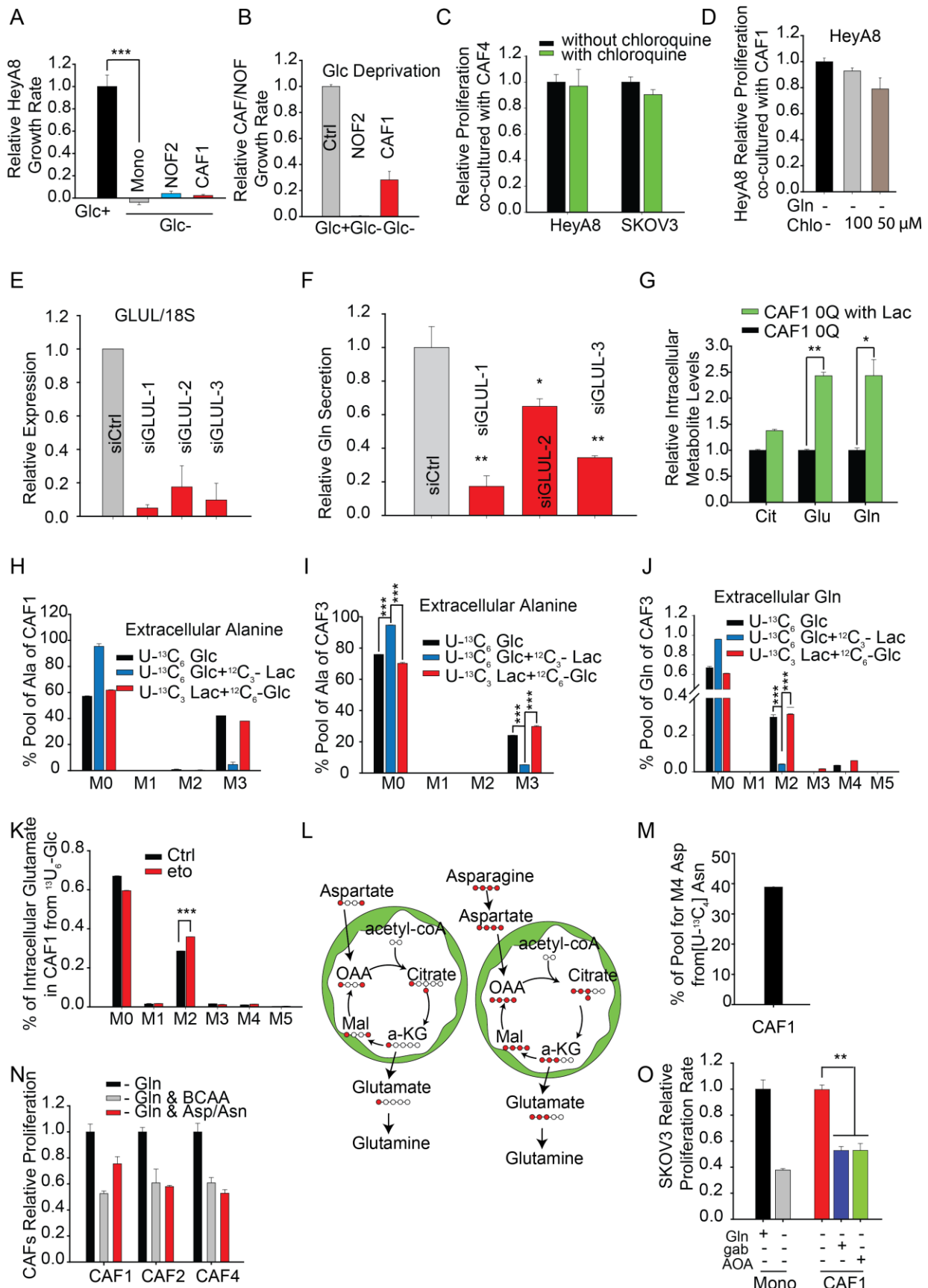


Figure S4, related to Figure 3, Figure 4, and Figure 5

(A): Growth rate of glucose-deprived HeyA8 co-cultured with NOF2 or CAF1 relative to mono-cultured HeyA8 in nutrient-rich medium. (B): Growth rate of NOF2 and CAF1 under glucose deprivation relative to nutrient-rich medium. (C): Proliferation rate of HeyA8 and SKOV3 co-cultured with CAF4 and treated with chloroquine relative to untreated HeyA8 or SKOV3. (D): Proliferation rate of HeyA8 co-cultured with CAF1 and treated with various concentrations of chloroquine relative to untreated HeyA8. (E): Expression of GLUL mRNA on transfection with three independent GLUL siRNA in CAF. (F): Relative Gln secretion rate with three independent GLUL siRNA in CAF. (G): Relative intracellular citrate, glutamate, Gln levels in Gln-deprived CAFs supplemented with lactate relative to Gln-deprived CAFs. (H-J): Mass isotopologue distributions (MIDs) of extracellular alanine (H) in CAF1 and alanine (I) and extracellular Gln (J) in CAF3 in presence of U-¹³C₆ Glucose or U-¹³C₃ Lactate labeled tracers. (K): Effect of etomoxir on the MID of intracellular glutamate in CAF1 in presence of U-¹³C₆ Glucose. (L): Schematic showing [1,4]-¹³C₂ Aspartate and U-¹³C₄ Asparagine enriching TCA cycle metabolites. (M): Percentage of U-¹³C₄ asparagine conversion into aspartate in CAF1. (N): Proliferation of CAF1,2,4 under Gln deprivation combined with removal of BCAAs or aspartate and asparagine from media relative to CAFs in only Gln-deprived medium. (O): Proliferation of SKOV3 co-cultured with CAF1 treated with Gabapentin (branch-chain aminotransferase, BCAT inhibitor) and AOA (aminotransferase inhibitor) relative to mono-cultured SKOV3 in Gln free medium. Error bars indicate mean ± s.e.m. for n≥3 independent experiments. Two tailed student t-test.

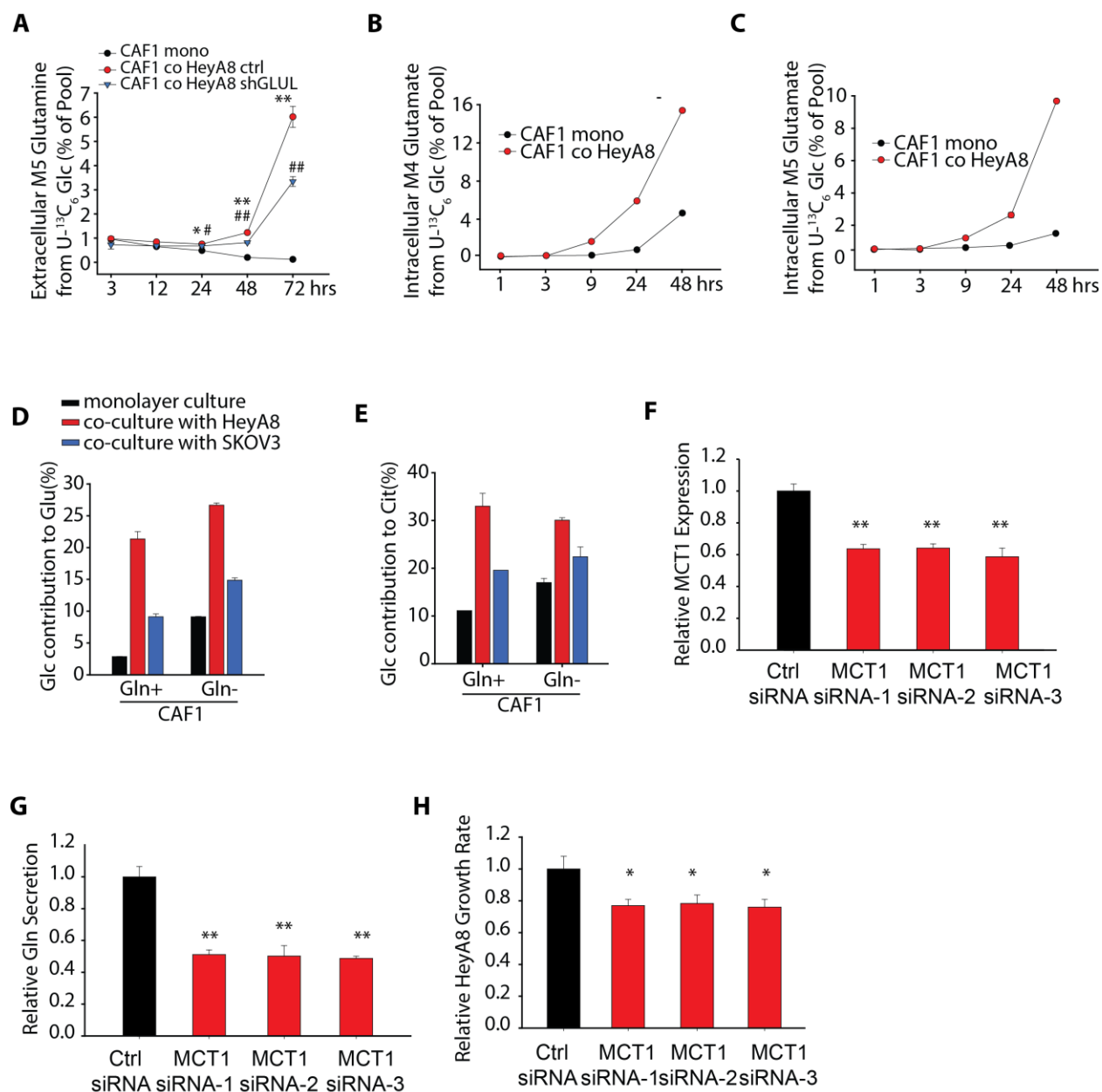


Figure S5, related to Figure 6:

(A) Dynamic isotope labeling of M5 Gln using U-¹³C₆ Glucose in CAF1 cultured with or without HeyA8 cells/ HeyA8 shGLUL. (B-C) Dynamic isotope labeling of M4 (B), M5 (C) glutamate using U-¹³C₆ Glucose in CAF1 cultured with or without HeyA8 cells. (D-E): Contribution of glucose to glutamate (D) and citrate (E) for CAFs when co-cultured with HeyA8 and SKOV3 under Gln deprivation condition. (F): Relative MCT1 expression level in CAF with three independent MCT1 siRNA. (G): Relative Gln secretion rate for CAF with three independent MCT1 siRNA. (H): Relative growth rate of HeyA8 cocultured with CAFs treated with MCT1 siRNA. Errors bars indicate mean \pm s.e.m. for $n \geq 3$ independent experiments. Two tailed student t-test.

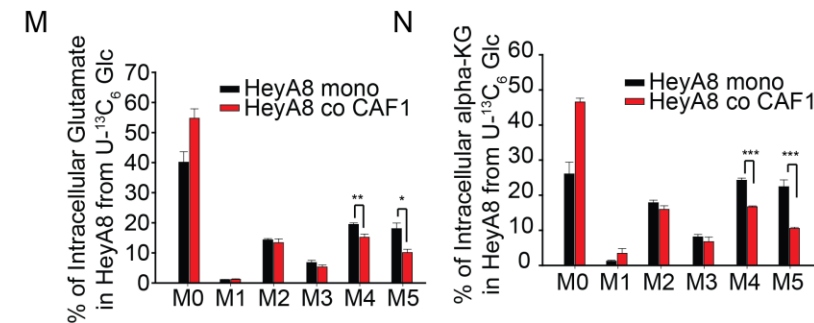
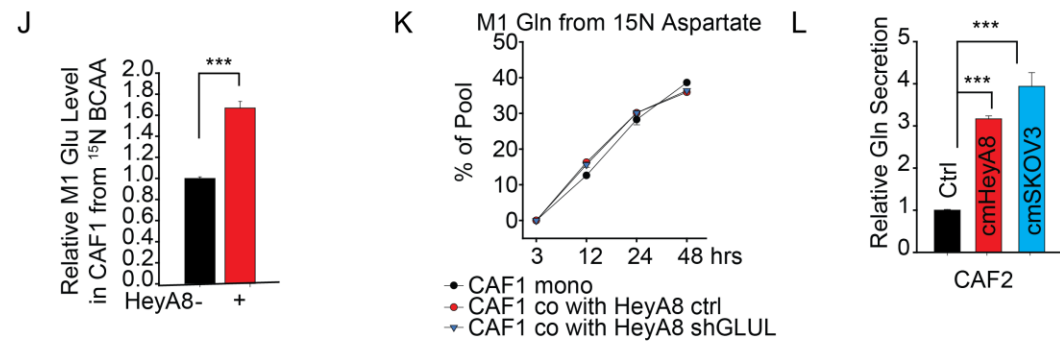
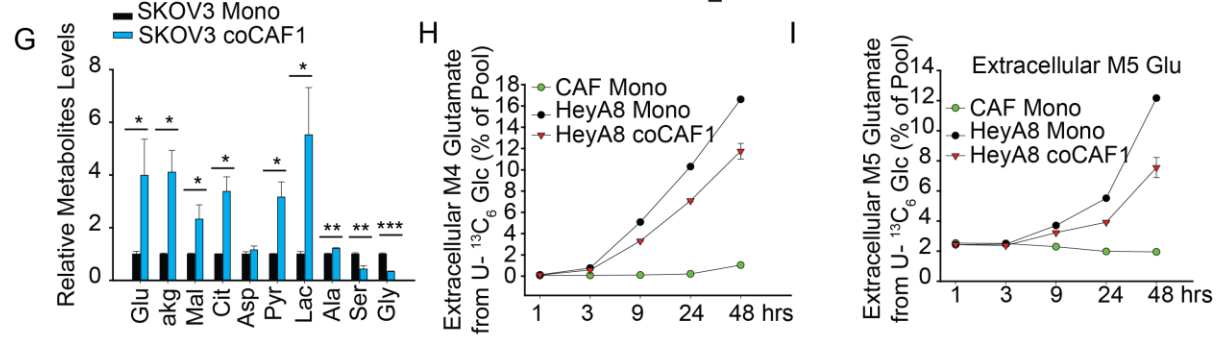
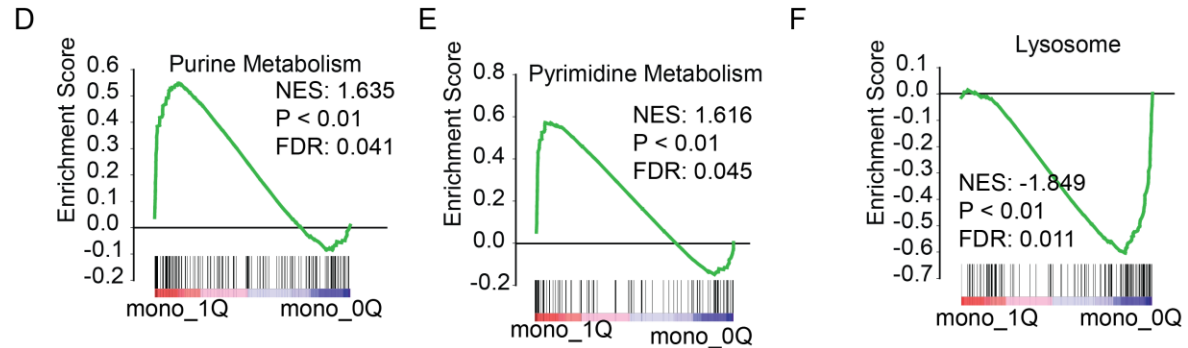
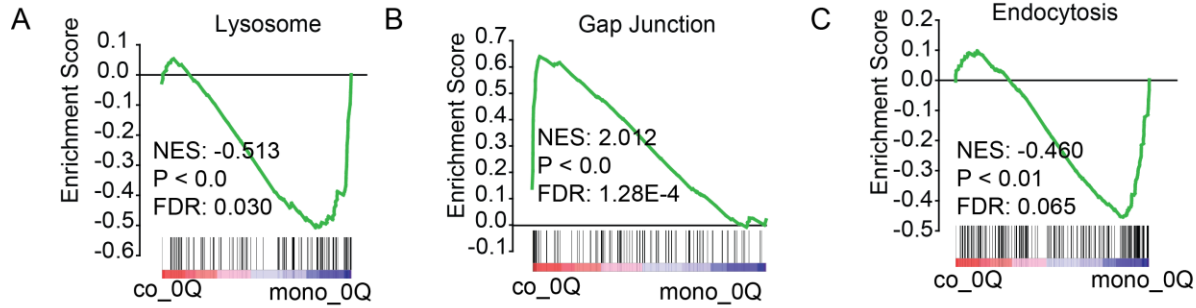
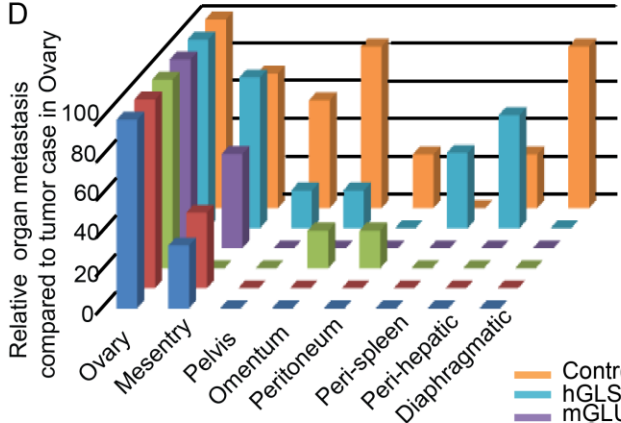
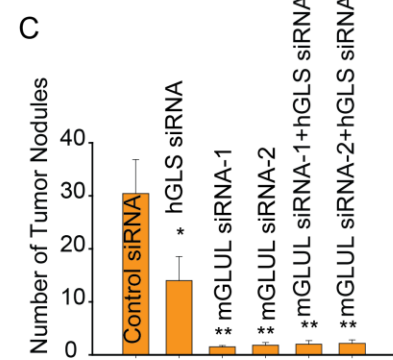
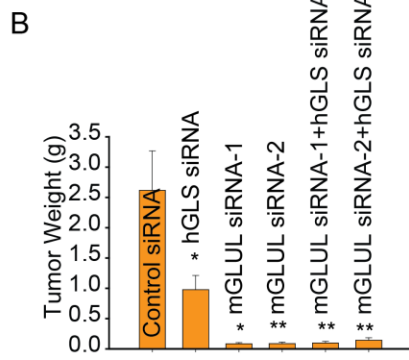
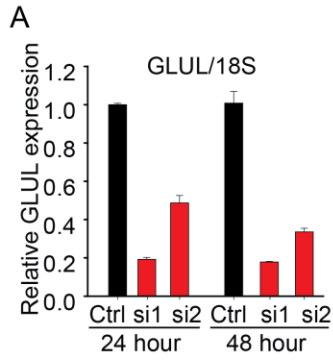


Figure S6: related to Figure 6

(A-C) GSEA of lysosome (A), gap junction (B) and endocytosis (C) regulating pathways in Gln-deprived HeyA8 co-cultured with CAF with respect to Gln-deprived HeyA8. (D-F): GSEA of purine (D), pyrimidine (E) synthesis and lysosome regulating (F) pathways in mono-cultured HeyA8 in Gln-rich medium with respect to HeyA8 in Gln-deprived medium. (G): Relative metabolite level for SKOV3 co-cultured with CAF1 relative to mono-cultured SKOV3. (H-I): Dynamic isotope labeling of M4 (H) and M5 (I) extracellular glutamate in spent media using U-¹³C₆ glucose in mono-cultured HeyA8 or CAF1 cultured with or without HeyA8. (J): Nitrogen contribution of ¹⁵N BCAA (leucine, isoleucine and valine) to intracellular glutamate (M1 isotopologue of glutamate) in CAF1 cultured with and without HeyA8. (K): Dynamic isotope labeling of extracellular M1 Gln using ¹⁵N Aspartate in CAF1 in mono-culture and co-cultured with HeyA8 or HeyA8 GLUL KD cells. (L): Effect of condition medium from OVCA on Gln secretion of CAF2. (M-N): Mass isotopologue distributions (MIDs) of intracellular glutamate (M) and α-ketoglutarate (N) from U-¹³C₆ glucose in HeyA8 cultured with and without CAF1. Errors bars indicate mean ± s.e.m. for n≥3 independent experiments. Two tailed student t-test.



E

WT cDNA 5'...CGGGCCTGCTTGTATGCTGGAGTCAAGATTACG...
 siRNA 3'CGAACAUACGACCUCAGUU
 MUT cDNA 5'...CGGGCCTGCTTGTATG**TACA**AGTCAAGATTACG...

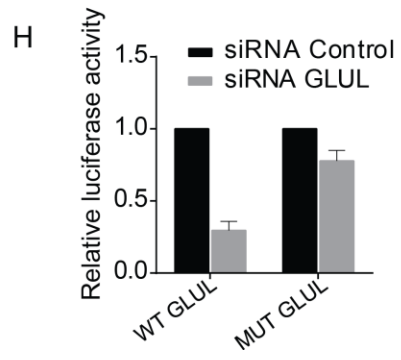
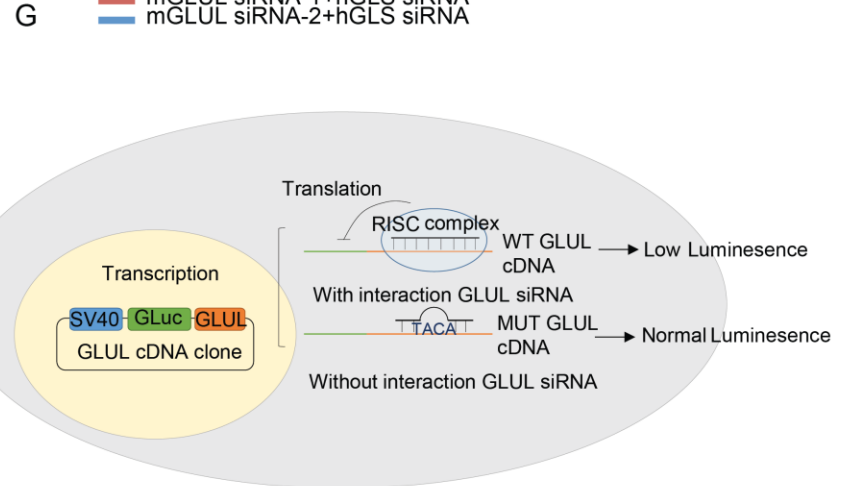
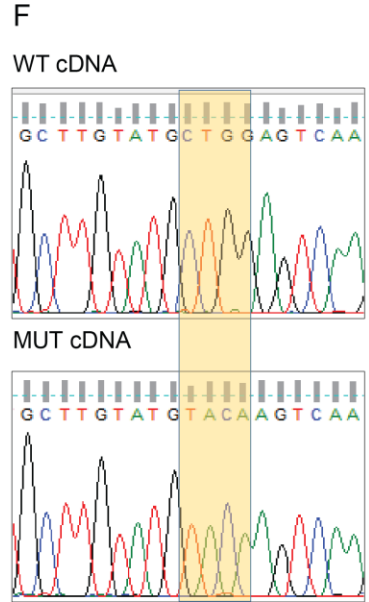


Figure S7, related to Figure 7:

(A): GLUL gene expression levels after transfection with mouse GLUL siRNA. (B): Using a well-characterized chitosan nanoparticle delivery system, mice were treated with control siRNA-CH, human GLS (hGLS) siRNA-CH, two independent murine GLUL (mGLUL) siRNA-CH and combination of hGLS + mGLUL siRNA-CH. $n > 4$ for each group. Weight of tumors extracted from mice subjected to control siRNA, human GLS siRNA, mouse GLUL siRNA and combination of hGLS and mGLUL siRNA. (C): Number of tumor nodules in mice subjected to control siRNA, human GLS siRNA, mouse GLUL siRNA and combination of hGLS and mGLUL siRNA. (D): Metastasis of ovarian tumor to different organ sites in mice treated with control siRNA, human GLS siRNA, murine GLUL siRNA and combination of hGLS and mGLUL siRNA. (E): Putative siRNA -1 GLUL binding site in the GLUL gene. (F): Sequence electropherograms of the wildtype and mutations. (G): Assay to determine whether siRNA targets a specific GLUL gene. (H): Luciferase activity in ID8 cells co-transfected with either WT- or Mut-GLUL reporter gene and control siRNA or GLUL siRNA. Renilla luciferase values normalized for firefly luciferase are presented. Errors bars indicate mean \pm s.e.m. for $n \geq 3$ independent experiments. Two tailed student t-test.

Supplementary Tables

Table S1, related to Figure 1:

Transcriptional factors for Gln anabolism pathway using Pathway Commons version 7.

from	type	to	source
FOXO3	controls-expression-of	GLUL	(van der Vos et al.)
GATA3	controls-expression-of	GLUL	(Kung et al., 2011)
AHR	controls-expression-of	HK2	PCv7
AR	controls-expression-of	GOT2	PCv7
ARNT	controls-expression-of	HK2	PCv7
ARNT	controls-expression-of	LDHA	PCv7
ATF1	controls-expression-of	LDHA	PCv7
ATF2	controls-expression-of	LDHA	PCv7
ATF3	controls-expression-of	LDHA	PCv7
CEBPA	controls-expression-of	GOT1	PCv7
CEBPB	controls-expression-of	GOT1	PCv7
CREB1	controls-expression-of	LDHA	PCv7
CREBBP	controls-expression-of	HK2	PCv7
CREBBP	controls-expression-of	LDHA	PCv7
CYP26A1	controls-expression-of	PDHB	PCv7
CYP26A1	controls-expression-of	SLC16A1	PCv7
E4F1	controls-expression-of	HK2	PCv7
EGR3	controls-expression-of	HK2	PCv7
ELK1	controls-expression-of	BCAT2	PCv7
EP300	controls-expression-of	HK2	PCv7

EP300	controls-expression-of	LDHA	PCv7
ESRRA	controls-expression-of	GOT1	PCv7
FOXA2	controls-expression-of	HK2	PCv7
GABPB2	controls-expression-of	BCAT2	PCv7
GTF2A2	controls-expression-of	BCAT2	PCv7
GTF3A	controls-expression-of	BCAT2	PCv7
HIF1A	controls-expression-of	HK2	PCv7
HIF1A	controls-expression-of	LDHA	PCv7
HNF4A	controls-expression-of	HK2	PCv7
HNF4A	controls-expression-of	SLC16A4	PCv7
LEF1	controls-expression-of	SLC16A1	PCv7
MAX	controls-expression-of	BCAT1	PCv7
MAX	controls-expression-of	LDHA	PCv7
MAZ	controls-expression-of	BCAT2	PCv7
MAZ	controls-expression-of	GOT1	PCv7
MAZ	controls-expression-of	LDHB	PCv7
MAZ	controls-expression-of	SLC16A4	PCv7
MYC	controls-expression-of	BCAT1	PCv7
MYC	controls-expression-of	LDHA	PCv7
MYC	controls-expression-of	SLC16A1	PCv7
NEUROD1	controls-expression-of	HK2	PCv7
NF1	controls-expression-of	GOT1	PCv7
NR3C1	controls-expression-of	GOT2	PCv7
PAX4	controls-expression-of	HK2	PCv7
PCBP1	controls-expression-of	HK2	PCv7
PDX1	controls-expression-of	HK2	PCv7
RREB1	controls-expression-of	GOT1	PCv7
SP3	controls-expression-of	LDHB	PCv7
SREBF1	controls-expression-of	HK2	PCv7
SRF	controls-expression-of	LDHA	PCv7

Table S2, related to Figure 2:

Intracellular fluxes of NOFs under Gln free medium, compared with Gln rich medium estimated using U-¹³C₆ Glucose tracer experiments and ¹³C-MFA

Reaction	SSE = 18.4, DOF = 15, Chi2(0.95) = [6.2, 27.4]			SSE = 11.8, DOF = 12, Chi2(0.95) = [4.4, 23.3]		
	Fluxes 1Q	95%CI LB	95%CI UB	Fluxes 0Q	95%CI LB	95%CI UB
GLU_C == AKG (net)	0.01	-0.02	0.08	-0.07	-0.14	0.04
GLU_C == AKG (exch)	1.00	0.65	1.00	0.53	0.29	0.53
CIT_M == AKG + CO2_out (net)	0.35	0.29	0.37	0.30	0.29	0.37
CIT_M == AKG + CO2_out (exch)	0.12	0.07	0.14	0.08	0.04	0.16
PYR_X == PYR_M (net)	0.04	0.01	0.08	0.07	0.00	0.15
PYR_X == PYR_M (exch)	0.04	0.00	0.06	0.12	0.05	0.18
0.5*SUC_M + 0.5*SUC_M == 0.5*FUM + 0.5*FUM (net)	0.34	0.30	0.38	0.18	0.14	0.30
0.5*SUC_M + 0.5*SUC_M == 0.5*FUM + 0.5*FUM (exch)	0.03	0.00	0.75	0.60	0.34	0.87
0.5*FUM + 0.5*FUM == MAL (net)	0.34	0.30	0.38	0.18	0.14	0.30
0.5*FUM + 0.5*FUM == MAL (exch)	1.00	0.97	1.00	0.30	0.27	0.41
MAL == OAC (net)	0.25	0.19	0.27	0.02	-0.09	0.08
MAL == OAC (exch)	1.00	0.93	1.00	0.94	0.00	1.00
GLN_C == GLU_C (net)	0.13	0.11	0.17	-0.04	-0.08	0.01
GLN_C == GLU_C (exch)	0.43	0.00	1.00	0.16	0.00	0.81
PYR_C == PYR_M (net)	0.30	0.14	0.35	0.31	0.19	0.41
PYR_C == PYR_M (exch)	0.56	0.51	0.61	0.37	0.30	0.48
GLN_X == GLN_C (net)	0.19	0.16	0.21	0.01	-0.01	0.02
GLN_X == GLN_C (exch)	0.24	0.05	0.34	0.13	0.00	1.00
GLU_X == GLU_C (net)	-0.08	-0.09	-0.06	-0.03	-0.03	-0.02
GLU_X == GLU_C (exch)	0.52	0.44	0.55	0.47	0.30	0.76
AS_X == AS_C (net)	0.02	0.00	0.04	0.05	0.02	0.08
AS_X == AS_C (exch)	0.12	0.04	0.14	0.00	0.00	0.03
OAC + GLU_C == AS_C + AKG (net)	-0.02	-0.04	0.00	-0.05	-0.08	-0.02
OAC + GLU_C == AS_C + AKG (exch)	0.32	0.00	1.00	0.71	0.00	1.00
GLC == G6P	1.00	0.92	1.04	0.96	0.92	1.05
G6P == PYR_C + PYR_C	1.00	0.92	1.04	0.96	0.92	1.05
PYR_C == LAC	1.70	1.63	1.74	1.61	1.53	1.71
PYR_M == ACCOA_M + CO2_out	0.35	0.29	0.37	0.30	0.29	0.37
OAC + ACCOA_M == CIT_M	0.35	0.29	0.37	0.30	0.29	0.37
AKG == 0.5*SUC_M + 0.5*SUC_M + CO2_out	0.34	0.30	0.38	0.18	0.14	0.30
MAL == PYR_M + CO2_out	0.09	0.06	0.16	0.16	0.08	0.37

0.5202*GLU_C+0.4339*GLN_C == BM	0.13	0.06	0.15	0.11	0.00	0.17
PYR_M + CO2_in == OAC	0.08	0.06	0.10	0.23	0.20	0.34
-GLC	1.00	0.92	1.04	0.96	0.92	1.05
LAC	1.70	1.63	1.74	1.61	1.53	1.71
-GLN_X	0.19	0.16	0.21	-0.01	-0.01	0.01
GLU_X	0.08	0.06	0.09	0.03	0.01	0.04
-AS_X	0.02	0.00	0.04	0.05	0.02	0.08
-PYR_X	0.04	0.01	0.08	0.07	0.00	0.15
BM	0.13	0.06	0.15	0.11	0.00	0.17

Table S3, related to Figure 2:

Intracellular fluxes of CAFs under Gln free medium, compared with Gln rich medium estimated using U-¹³C₆ Glucose tracer experiments and ¹³C-MFA

Reaction	SSE = 15.3, DOF = 14, Chi2(0.95) = [5.6, 26.1]			SSE = 22.0, DOF = 13, Chi2(0.95) = [5.0, 24.7]		
	Fluxes 1Q	95%CI LB	95%CI UB	Fluxes 0Q	95%CI LB	95%CI UB
GLU_C == AKG (net)	0.13	0.11	0.29	0.08	0.06	0.14
GLU_C == AKG (exch)	1.00	0.25	1.00	0.41	0.36	0.44
CIT_M == AKG + CO2_out (net)	0.21	0.16	0.26	0.27	0.25	0.30
CIT_M == AKG + CO2_out (exch)	0.11	0.05	0.18	0.14	0.09	0.19
PYR_X == PYR_M (net)	-0.03	-0.08	0.00	0.08	0.05	0.14
PYR_X == PYR_M (exch)	0.15	0.00	0.22	0.02	0.00	0.03
0.5*SUC_M + 0.5*SUC_M == 0.5*FUM + 0.5*FUM (net)	0.30	0.25	0.45	0.25	0.22	0.27
0.5*SUC_M + 0.5*SUC_M == 0.5*FUM + 0.5*FUM (exch)	0.38	0.00	1.00	0.01	0.00	0.03
0.5*FUM + 0.5*FUM == MAL (net)	0.30	0.25	0.45	0.25	0.22	0.27
0.5*FUM + 0.5*FUM == MAL (exch)	1.00	0.90	1.00	1.00	0.98	1.00
MAL == OAC (net)	0.17	0.10	0.20	0.16	0.11	0.18
MAL == OAC (exch)	1.00	0.97	1.00	1.00	0.99	1.00
GLN_C == GLU_C (net)	0.14	0.12	0.20	-0.02	-0.02	-0.02
GLN_C == GLU_C (exch)	0.65	0.24	0.83	0.36	0.32	0.38
PYR_C == PYR_M (net)	0.11	-0.08	0.17	0.11	0.02	0.14
PYR_C == PYR_M (exch)	0.24	0.18	0.29	0.22	0.17	0.27
GLN_X == GLN_C (net)	0.16	0.13	0.20	-0.02	-0.02	-0.02
GLN_X == GLN_C (exch)	0.25	0.17	0.32	0.17	0.13	0.19
GLU_X == GLU_C (net)	-0.03	-0.04	-0.02	0.00	0.00	0.00
GLU_X == GLU_C (exch)	0.51	0.47	0.57	0.47	0.45	0.50
AS_X == AS_C (net)	0.04	0.02	0.10	0.11	0.09	0.16
AS_X == AS_C (exch)	0.13	0.00	0.52	0.24	0.14	0.27

OAC + GLU_C == AS_C + AKG (net)	-0.04	-0.10	-0.02	-0.11	-0.16	-0.09
OAC + GLU_C == AS_C + AKG (exch)	1.00	0.00	1.00	0.60	0.55	0.63
GLC == G6P	1.01	0.83	1.08	0.96	0.85	1.00
G6P == PYR_C + PYR_C	1.01	0.83	1.08	0.96	0.85	1.00
PYR_C == LAC	1.90	1.74	2.01	1.80	1.68	1.86
PYR_M == ACCOA_M + CO2_out	0.21	0.16	0.26	0.27	0.25	0.30
OAC + ACCOA_M == CIT_M	0.21	0.16	0.26	0.27	0.25	0.30
AKG == 0.5*SUC_M + 0.5*SUC_M + CO2_out	0.30	0.25	0.45	0.25	0.22	0.27
MAL == PYR_M + CO2_out	0.13	0.11	0.29	0.08	0.06	0.14
0.5202*GLU_C+0.4339*GLN_C == BM	0.04	0.00	0.31	0.00	0.00	0.00
-GLC	1.01	0.83	1.08	0.96	0.85	1.00
LAC	1.90	1.74	2.01	1.80	1.68	1.86
-GLN_X	0.16	0.13	0.20	0.02	0.02	0.02
GLU_X	0.03	0.01	0.04	0.00	0.00	0.00
-AS_X	0.04	0.02	0.10	0.11	0.09	0.16
PYR_X	0.03	0.00	0.08	0.08	0.05	0.14
BM	0.04	0.00	0.31	0.00	0.00	0.00

Table S4, related to Figure 2:

Intracellular fluxes of CAFs and NOFs under Gln free medium (normalized with flux of pyruvate into TCA cycle) estimated using U-¹³C₆ Glucose tracer experiments and ¹³C-MFA

	NOF Glutamine Deprived	CAF Glutamine Deprived
Reaction	NOF 0Q	CAF 0Q
GLU_C == AKG (net)	-0.24	0.78
CIT_M == AKG + CO2_out (net)	0.99	2.50
PYR_X == PYR_M (net)	0.23	0.72
0.5*SUC_M + 0.5*SUC_M == 0.5*FUM + 0.5*FUM (net)	0.59	2.27
0.5*FUM + 0.5*FUM == MAL (net)	0.59	2.27
MAL == OAC (net)	0.07	1.50
GLN_C == GLU_C (net)	-0.13	-0.23
PYR_C == PYR_M (net)	1.00	1.00
GLN_X == GLN_C (net)	0.03	-0.23
GLU_X == GLU_C (net)	-0.08	0.00
AS_X == AS_C (net)	0.16	1.01
OAC + GLU_C == AS_C + AKG (net)	-0.16	-1.01
GLC == G6P	3.13	8.86
G6P == PYR_C + PYR_C	3.13	8.86
PYR_C == LAC	5.26	16.72

PYR_M == ACCOA_M + CO2_out	0.99	2.50
OAC + ACCOA_M == CIT_M	0.99	2.50
AKG == 0.5*SUC_M + 0.5*SUC_M + CO2_out	0.59	2.27
MAL == PYR_M + CO2_out	0.52	0.78
0.5202*GLU_C+0.4339*GLN_C == BM	0.37	0.00
PYR_M + CO2_in == OAC	0.76	
-GLC	3.13	8.86
LAC	5.26	16.72
GLN_X	-0.03	0.23
GLU_X	0.08	0.00
-AS_X	0.16	1.01
-PYR_X	0.23	0.72
BM	0.37	0.00
GLUD1 (GLU -> AKG)	-0.08	1.79
PYR_C -> PYR_M (net)	0.79	0.17

Supplementary Experimental Procedures:

Cells and reagents. SKOV3, HeyA8 were purchased from ATCC on behalf of Rice University. Ovarian CAFs were derived from advanced stage high-grade serous ovarian cancer samples and normal ovarian fibroblasts (NOFs) were derived from normal ovaries obtained from patients with benign gynecologic malignancies. Both CAFs and NOFs were kindly provided by Dr. Jinsong Liu and Dr. Samuel Mok from MD Anderson. All tissue samples were collected under the approval of the institution review board (IRB). Dialyzed FBS was purchased from Invitrogen. Stable Isotopes were purchased from Cambridge Isotopes Laboratories. 6 well inserts were purchased from Corning.

Cell culture. Ovarian cancer cells were cultured in RPMI 10% fetal bovine serum (Sigma Aldrich), 100U/ml penicillin and 100 U/ml streptomycin. Primary CAFs cultures were derived from tumor tissues resected from high grade serous ovarian cancer patients. Patient-derived CAFs cultures were evaluated by immunofluorescent microscopy and confirmed the expression of CAFs-specific markers including alpha smooth muscle actin (α -SMA) and fibroblast activation protein (FAP). Ovarian cancer associated fibroblasts cells were cultured in 1:1 mixture of MCDB105 (Sigma Aldrich) and M199 (Invitrogen) supplemented with 15% fetal bovine serum (Sigma Aldrich), 1ng/ml epidermal growth factor (EGF, Sigma Aldrich) and were used at low passage for the described experiments. All cells were incubated in 5% CO₂, and 37°C incubator.

Proliferation assay. CAFs were seeded in 96 well plates, and after the attachment, seed GFP labeled ovarian cancer cells overnight. Medium were changed to different nutrients conditions or with different drugs. Fluorescence value were measured at 480/515 nm.

Glucose assay. Glucose assay were done according to the instructions of assay kit (Wako Glucose kit). In brief, Samples were diluted in PBS (1:10), and mixed with plated reader. 200 μ l of reconstituted Wako glucose reagent was added to a 96-well assay plate followed with 10 μ l sample dilution in each well. The plate was incubated at 37°C for 15 min. Absorbance was measured at 505 nm and 600 nm by using a spectrophotometer (SpectraMax M5; Molecular Devices).

Lactate assay. Lactate secretion was determined using the Trinity Lactate Kit. Medium samples were diluted in PBS (1:10), and mixed with plated reader. Lactate reagent was reconstructed and added with 10 μ l diluted samples in an assay plate. The plate was incubated for 1 h at 37°C. Absorbance was read on a spectrophotometer at 540 nm.

Protein assay. Protein assays are used to do normalization in our experiment and is done according to Bicinchoninic Acid Protein Assay protocol (Thermo Fisher). In brief, 200 μ l protein reagent was added to a 96-well assay plate and mix with samples or standard, and then incubated at 37°C for 30 min. The absorbance was read on a spectrophotometer at 562 nm.

Amino acid uptake. Ultra-high-performance liquid chromatography (UPLC) was used to assess amino acid uptake and secretion using Waters Acquity UPLC device. Briefly, media samples were deproteinized, and MassTrak Reagent was added to the samples, along with Borate Buffer/NaOH. Samples were then heated and analyzed using the Waters ACQUITY UPLC system. Eluents were prepared according to Waters' protocol. MassTrak AAA eluent A concentrate was diluted 1:10 in milliQwater, and MassTrak AAA eluent B was inputted in undiluted form. Flow rate of eluents was 0.4 ml/min, and UV detection was at 260 nm.

Average gene expression of pathways analysis

Genes for Gln anabolism pathway include GLUL, GLUD1/2, 2, GPT, BCAT1/2. Genes for glycolysis pathway include ACSS1/2, ADH1A, ALDH2, DLAT, ENO1, GAPDH, GPI, HI1, LDHA/B/C, PCK1, PFKL/M/P, PGAM1, PGM1, PGK1, TII1, PKM, SLC16A1, SLC16A3. To analyze the pathway gene expression level, average gene expression is calculated for all involved genes for one sample, and average value represents this sample's average gene expression of pathway.

RNA purification and amplification for Illumina Microarrays. Cells were seeded in 6 well plates, and RNA was extracted using the Quick-RNATM MiniPrep. RNA amplification was carried by Illumina® TotalPrepTM RNA amplification kit, according to manufacture instructions. HumanHT-12 v4 Expression BeadChip Kit (Illumina) was used for hybridization and imaging, according to manufacturer's protocol

GLS, GLUL and MCT1 gene silencing by small interfering RNA

Small interfering RNA (siRNA) targeted to GLS, GLUL, MCT1, mGLUL was purchased from Sigma. In vitro transient transfection was performed as described previously (Landen et al., 2005). Briefly, cells were transfected with GLUL specific or scrambled (control) siRNA using lipofectamine reagent (Invitrogen, Carlsbad, CA). Cells were harvested at selected time

intervals, to measure mRNA levels of GLUL using quantitative reverse transcriptase-PCR (qRT-PCR).

Quantitative real-time RT-PCR

Total RNA was isolated using Qiagen RNeasy kit (Qiagen). cDNA was synthesized using the Superscript™ First-strand kit (Invitrogen) as per the manufacturer's instructions. Real-time qRT-PCR was performed using a 7000 Sequence Detection System (Applied Biosystems, Foster City, CA) with the SYBR® GreenERTM qPCR Supermix kit (Invitrogen, Carlsbad, CA) as per the manufacturer's instructions.

Primers:

Genes	Forward	Reverse
GLUL	CCTGCTTGTATGCTGGAGTC	GATCTCCCATGCTGATTCCCT
CDC2	TGGATCTGAAGAAATACTTGGATTCTA	CAACCCCTGTAGGATTTGG
CDK2	ACCAGCTCTTCCGGATCTTT	CATCCTGGAAGAAAGGGTGA
CDC45	TTCGTGTCCGATTTCCGCAA	TGGAACCAGCGTATATTGCAC
MCM4	GACGTAGAGGCGAGGATTCC	GCTGGGAGTGCCGTATGTC
BUB1	TGGGAAAGATACATACAGTGGGT	AGGGGATGACAGGGTTCCAAT
BCL-xl	CGTGGAAGCGTAGACAA	GTGGGAGGGTAGAGTGGAT
BCL2	CATGCTGGGGCCGTACAG	GAACCGGCACCTGCACAC
ATFM1	TTCCAGCGATGGCATGTTCC	TCCTACTGTTGATAAGCCCACA
MCL1	GCCAAGGACACAAAGCCAAT	AACTCCACAAACCCATCCCA
MCT1	GTGGCTCAGCTCCGTATTGT	GAGCCGACCTAAAAGTGGTG
18S	AGAAACGGCTACCACATCCAA	GGGTCTGGGAGTGGGTAAATTT
mGLUL	CCGCCTCGCTCTCCTGACC	CGGGTCTTGCAGCGCAGTC

Transcriptional Factors Analysis

The transcription factor - target gene interaction data were downloaded from pathway commons version 7 (Cerami et al., 2011). All binary interaction data were downloaded and then filtered to include only the interaction type 'controls-expression-of'. FOXO3 and GATA3 are from recent published papers. Detail information is presented in Supplementary Table 2.

In-vivo models and tissue processing

Female athymic nude mice were purchased from the National Cancer Institute, Frederick Cancer Research and Development Center (Frederick, MD) and maintained according to guidelines set forth by the American Association for Accreditation of Laboratory Animal Care and the US Public Health Service policy on Human Care and Use of Laboratory Animals. All mouse studies were approved and supervised by the MD Anderson Cancer Center Institutional Animal Care and Use Committee. All animals used were between 8 and 12 weeks of age at the time of injection. To determine the therapeutic efficacy of GLS and GLUL gene silencing, we used well characterized orthotopic model of ovarian carcinoma. To establish the tumors, SKOV3ip1 ovarian cancer cells (750,000) were trypsinized and suspended in 50 µl of Hanks balanced salt solution (HBSS; Gibco, Carlsbad, CA) and injected directly into the left ovary of anaesthetized female nude through a 1.5-cm intraperitoneal incision. Seven days after cell injection, mice were randomly divided into 4 groups: 1) CH/Control siRNA 2) CH/hGLS siRNA or 3) CH/ mGLUL siRNA-1, 4) CH/hGLS + mGLUL siRNA-1, 5) CH/ mGLUL siRNA-2, or 6)

CH/hGLS + mGLUL siRNA-1. To assess tumor growth, treatment began by injecting CH/siRNA nanoparticles twice weekly (150 µg/kg body weight) through intravenous injection. Mice were monitored daily for adverse effects of therapy and were sacrificed when they became moribund (6-7 weeks after cell injection). At the time of sacrifice, mouse weight and tumor weight was recorded. Tumor tissue was harvested and either fixed in formalin for paraffin embedding, or frozen in optimum cutting temperature medium (OCT; Miles, Inc., Elkhart, IN) to prepare frozen slides, or snap-frozen in liquid nitrogen for lysate preparation. The individuals who performed the necropsies, tumor collections, and tissue processing were blinded to the treatment group assignments.

Interstitial Fluid Extraction from Mice Tumors

Tumors were excised from the mice, flushed with saline to remove blood from the surface, and blotted gently with tissue paper to remove excess saline. Next, we used a nylon mesh with pore size ~15×20 µm as a basket in the 2ml tube and to measure tumor weight within a range of 0.25 to 1.0 gram, then transferring the intact tumor into the tube. Tubes were immediately capped, and spun in an Eppendorf 5417R centrifuge placed in a cold room maintained at 4°C. Initial speed was set to 500 rpm (27g) for 10 mins, if no fluid was observed at the bottom, speed was increased by 100-rpm and centrifuged for another 10 mins. Usually the fluid appeared at speeds of 800 rpm (68g). Interstitial fluid was collected for further analysis and the solid tumors were transferred to another tube and centrifuged at 1000 rpm (106g) for 10 mins. Additional fluid was collected and tubes containing solid tumors were centrifuged at 2000 rpm (424g). The collected fluid samples were analyzed for glucose and lactate concentration.

Immunohistochemistry

Paraffin-embedded tumor sections were heated, deparaffinized, and antigen retrieval was performed by steaming, and endogenous peroxides were blocked with 3% hydrogen peroxide in methanol. Nonspecific proteins were blocked with 4% fish gelatin in PBS. Slides were incubated in primary antibody (1:100), and the secondary antibody (ready-to-use) was followed by streptavidin horseradish peroxidase (ready-to-use). Slides were quantified by counting the number of positively staining cells per 200× field.

DNA constructs

To generate pLight-GLUL, DNA fragments encoding *GLUL* were amplified from murine ovarian cancer ID8 cells using the primer set: 5'- GCTCTAGAGTTCCCACTTGAACAAAGG -3' and 5'- GCCTCGAGGTTACAGTGGGGACAAC -3'. Amplified DNA was cloned into the *Xba*I/*Xho*I sites of the pLightSwitch_3UTR (Switchgear Genomics). Plasmid integrity was verified by DNA sequencing.

Site-directed mutagenesis

Q5® Site-Directed Mutagenesis Kit was used (New England BioLabs) according to the manufacturer's instructions. To create mutations in the siRNA-binding site of *GLUL* gene, the following primers were used: TACA, 5'- TGCTTGATGtacaAGTCAAGATTACGGGGACAAATG -3' (forward) and 5'- GGCCCGGTAGTGAGCCTC -3' (reverse). Thermal cycling conditions for PCR were 98°C for 30 seconds; 25 cycles of 98°C for 10 seconds, 60°C for 30 seconds, and 72°C for 6 minutes; and 72°C for 2 minutes. PCR products were digested with *KLD* at room

temperature for 5 minutes and transformed into NEB® 5-alpha competent bacterial cells (New England BioLabs). Mutations were verified by DNA sequencing.

Luciferase enzymatic assay

ID8 cells were maintained in DMEM with 10% FBS and seeded at 10^5 cells per well in 12-well plates 1 day prior to the assay. Cells were administered using Lipofectamine 2000 (Invitrogen) with 200 ng *WT*- or *Mut-GLUL* reporter, together with 100pmol *siRNA Control* or *siRNA GLUL* and 50 ng PRL-CMV plasmid to normalize transfection efficiency. After 24 hours, cells were washed with PBS and permeabilized with Cell Culture Lysis Reagent (Promega). Dual-Luciferase activity was measured with a Turner Biosystems TD-20/20 luminometer after addition of 50 μ l luciferase assay reagent and 50 μ l Stop&Glo reagent (Promega).

¹³C Metabolic Flux Analysis

Flux analysis was performed using a MATLAB-based software developed within our lab using KNITRO® optimization toolbox. ¹³C atom transitions were modeled according to the Atom Mapping Matrix (AMM) (Zupke and Stephanopoulos, 1994) and Isotopomer Mapping Matrix (IMM) (Schmidt et al., 1997) method. Reversible reactions were modeled as two irreversible forward and reverse fluxes (v_{fwd}, v_{rev}) and transformed into net and normalized exchange fluxes (v_{net}, \tilde{v}_{xch}) (Wiechert and deGraaf, 1997; Wiechert et al., 1997) are described by equations (1) to (3).

$$v_{net} = v_{fwd} - v_{rev} \dots (1)$$

$$v_{xch} = \min(v_{fwd}, v_{rev}) \dots (2)$$

$$\tilde{v}_{xch} = \frac{v_{xch}}{v_{xch} + \beta} \dots (3)$$

β is a constant chosen in the order of magnitude of net fluxes. Since we normalize all net fluxes with respect to glucose uptake we choose a value of $\beta = 2$. Mass balance of intracellular metabolites is applied assuming pseudo steady-state because most intracellular metabolites have a high turnover rate of intracellular pools. The stoichiometric matrix S , is formed according to the metabolic model and the equation for mass balance for vector $v = [v_{net}, v_{boundary}]$ becomes equation (4).

$$Sv = 0 \dots (4)$$

AMMs and IMMs are used to generate carbon atom balances for each reactant-product in every reaction in the metabolic network. In addition to the flux variables v , isotopomer distribution vectors (IDVs, represented by vector y) are used to describe mass isotopomer fractions of intracellular metabolites.

$$x = [v, y] \dots (5)$$

The isotopomer mass balances derived using IMMs are non-linear since the rate of production of isotopomers is proportional to the flux and mass isotopomers of precursor metabolites. The mass balance of metabolite B will therefore be

$$c_B \frac{dy^B}{dt} = 0 = v_{A \rightarrow B} \cdot (IMM_{A \rightarrow B} \times y^A) - v_{B \rightarrow} \cdot y^B \dots (6)$$

Assuming measurements are made after isotopic steady-state is reached, the general form of the isotopomer mass balance equations for metabolite i, over all N reactions can be represented as

$$f_i(x) = \sum_{j=1}^N S_{ij} \cdot v_j \left(\prod_{\substack{S_{ij} > 0 \\ k: S_{kj} < 0}} IMM_{k \rightarrow i} \cdot y^i \right) + \sum_{j=1, S_{ij} < 0}^N S_{ij} \cdot y^i = 0 \dots (7)$$

To solve the equations (4) and (7) for the flux distribution of metabolic network, minimizing the variance weighted sum of square of errors between measured quantities and unknown variables in the system. We convert the IDV to respective mass isotopologue distributions (MIDs) in order to compute error between model and measurements from GC-MS.

Metabolic model and data processing

Flux analysis was conducted on CAFs and NOFs labeled with U-13C6-Glucose under nutrient-rich media (1Q) and glutamine (0Q) conditions. The metabolic model contained 30 and 21 metabolites involved in glycolysis, TCA cycle and glutamine pathways. MID measurements obtained from GC-MS for glutamate, α -ketoglutarate, fumarate, malate, citrate, pyruvate and lactate are used for 13C-MFA. MIDs are corrected for natural abundance using IsoCor (Millard et al., 2012) before used in 13C-MFA. Fluxes in the model are bounded by extracellular fluxes obtained for glucose and glutamine uptake and lactate secretion.

Global optimum solution for 13C-MFA is obtained by solving the minimization from at least 50 randomly generated initial guess vectors. Veracity of the solution is checked using the χ^2 goodness-of-fit test for parameter fitting problems. Furthermore, 95% confidence intervals for fluxes are estimated by performing Monte Carlo simulations. For MC simulations, at least 500 samples are generated by introducing normally distributed random error to measurements and the 13C-MFA problem is solved for each sample. Lower and upper bounds of the confidence intervals for each flux are selected from the 500 normally distributed solutions which lie within probability of 0.025 and 0.975, respectively. 500 samples were chosen for MC simulations after performing the MC simulations for 100, 250, 500, 750 and 1000 perturbations. Confidence interval ranges did not change significantly for more than 500 samples in the CAF 1Q condition.

Linear Regression analysis for estimating percentage contribution of extracellular CAF-secreted Gln to intracellular glutamate in OVCA. We assumed that the intracellular glutamate in OVCA under co-culture system is generated by metabolizing extracellular Gln secreted by CAFs and intracellular glutamate synthesis from glucose via TCA cycle. It is also assumed that OVCA do not uptake extracellular glutamate. We formulate an equation to balance the mass isotopologue distributions (MIDs)

$$M_i^{(final\ product)} = x * M_i^{(source\ 1)} + y * M_i^{(source\ 2)}$$

For intracellular glutamate in CAFs described for Fig. 6j, the equation is formed as,

$$M_i^{(int\ Glu, CAF)} = x * M_i^{(ext\ Glu)} + y * M_i^{(int\ Cit, CAF)}$$

For glutamate in shared coculture media described for Fig. 6k, the equation is formed as,

$$M_i^{(ext\ Glu)} = x * M_i^{(int\ Glu,OVCA)} + y * M_0^{(prior\ Glu,media)}$$

For intracellular glutamate in OVCA cells described for Fig. 7m, the equation is formed as,

$$M_i^{(int\ Glu,OVCA)} = x * M_i^{(ext\ Glu)} + y * M_i^{(int\ Cit,OVCA)}$$

It was assumed that intracellular citrate was the precursor for endogenous glutamate synthesis and extracellular glutamate in cancer cells co-cultured with CAF, and extracellular Gln MID to estimate the contribution of CAF-secreted Gln on glutamate synthesis in cancer cells. We used measured MID of extracellular Gln, along with intracellular glutamate and citrate for the model.

Here, M_i represents different mass isotopologue which is i units heavier than unlabeled species. x represents the percentage contribution of source 1 to final product in OVCA, y represents the percentage contribution of source 2 to final product. Take final product as intracellular glutamate, source 1 as intracellular citrate, source 2 as extracellular glutamine as example, M_0 intracellular glutamate can be generated by M_0 intracellular citrate and M_0 extracellular Gln; M_2 intracellular glutamate can be generated by M_2 intracellular citrate and M_2 extracellular Gln; M_4 intracellular glutamate can be generated by M_4 intracellular citrate and M_4 extracellular Gln; M_5 intracellular glutamate can be generated by M_5+M_6 intracellular citrate and M_5 extracellular Gln. Using a two-variable and two parameter linear regression for M_0 , M_2 , M_4 , M_5 of glutamate, we estimate the value for x and y .

Data Resources:

GSE40595, GSE 87773

Statistical analysis. Comparison of the data sets obtained from the different experiment conditions was performed with the two tailed student t test. In the bar graphs, data is shown as mean \pm s.e.m., single asterisk (*) represents $P < 0.05$, double asterisks (**) represent $P < 0.01$ and triple asterisks (***) represent $P < 0.001$.

References:

- Cerami, E.G., Gross, B.E., Demir, E., Rodchenkov, I., Babur, O., Anwar, N., Schultz, N., Bader, G.D., and Sander, C. (2011). Pathway Commons, a web resource for biological pathway data. *Nucleic Acids Res* 39, D685-690.
- Kung, H.N., Marks, J.R., and Chi, J.T. (2011). Glutamine Synthetase Is a Genetic Determinant of Cell Type-Specific Glutamine Independence in Breast Epithelia. *Plos Genetics* 7.
- Landen, C.N., Jr., Chavez-Reyes, A., Bucana, C., Schmandt, R., Deavers, M.T., Lopez-Berestein, G., and Sood, A.K. (2005). Therapeutic EphA2 gene targeting in vivo using neutral liposomal small interfering RNA delivery. *Cancer research* 65, 6910-6918.
- Millard, P., Letisse, F., Sokol, S., and Portais, J.C. (2012). IsoCor: correcting MS data in isotope labeling experiments. *Bioinformatics* 28, 1294-1296.
- Schmidt, K., Carlsen, M., Nielsen, J., and Villadsen, J. (1997). Modeling isotopomer distributions in biochemical networks using isotopomer mapping matrices. *Biotechnology and Bioengineering* 55, 831-840.

van der Vos, K.E., Eliasson, P., Proikas-Cezanne, T., Vervoort, S.J., van Boxtel, R., Putker, M., van Zutphen, I.J., Mauthe, M., Zellmer, S., Pals, C., Verhagen, L.P., Groot Koerkamp, M.J., Braat, A.K., Dansen, T.B., Holstege, F.C., Gebhardt, R., Burgering, B.M., and Coffey, P.J. Modulation of glutamine metabolism by the PI(3)K-PKB-FOXO network regulates autophagy. *Nat Cell Biol* 14, 829-837.

Wiechert, W., and deGraaf, A.A. (1997). Bidirectional reaction steps in metabolic networks .1. Modeling and simulation of carbon isotope labeling experiments. *Biotechnology and Bioengineering* 55, 101-117.

Wiechert, W., Siefke, C., deGraaf, A.A., and Marx, A. (1997). Bidirectional reaction steps in metabolic networks .2. Flux estimation and statistical analysis. *Biotechnology and Bioengineering* 55, 118-135.

Zupke, C., and Stephanopoulos, G. (1994). Modeling of Isotope Distributions and Intracellular Fluxes in Metabolic Networks Using Atom Mapping Matrices. *Biotechnology Progress* 10, 489-498.